Thermal Profile and Microstructure Analysis of Al-Si with the Magnesium Addition under Different Cooling Conditions

M. F. M. Tajudin[1], *A. H. Ahmad[1,2], J. Alias[1,2], N. A. Abd Razak[1], S. Naher[3]

[1]*Faculty of Mechanical and Automotive Engineering Technology, Universiti Malaysia Pahang Al-Sultan Abdullah, 26600 Pekan, Pahang, Malaysia*
[2]*Centre for Automotive Engineering, Universiti Malaysia Pahang Al-Sultan Abdullah, 26600 Pekan, Pahang, Malaysia.*
[3] *Department of Mechanical Engineering and Aeronautics, City University of London, London EC1V 0HB, UK.*

**asnul@umpsa.edu.my*

Abstract

Thermal analysis is an effective approach for studying the characteristics of materials under different temperature situations. The study implemented cooling curve analysis (CCA), complemented by computational methods for precisely evaluating the temperature variation of the molten alloy by employing two thermocouples. An aluminium alloy with 1 wt. % Mg addition was melted in graphite crucible and subjected to various cooling conditions, which included normal, slow, fast, and fastest cooling rate conditions. Normal cooling condition (A) was achieved when the crucible was allowed to cool down to room temperature. Meanwhile, the slow cooling condition (B) was achieved when the crucible was allowed to cool within the Kaowool insulator chamber. In addition, the fast (C) and fastest (D) cooling conditions were attained when the forced airflow was directed at the crucible at minimum and maximum speed, respectively. The temperature data was collected via K-type thermocouples connected to a Ni 9129 data acquisition system and DasyLab software. Cooling curves, cooling curves with baselines, dendritic coherency points, and solid fractions were then recorded using OriginPro 2019b software. The liquidus, eutectic, and solidus temperatures were determined. The microstructure of the alloy sample was characterised by optical microscopy (OM), scanning electron microscopy (SEM), combined with energy dispersive X-ray spectroscopy (EDX), and X-ray diffraction (XRD) analysis. The results show that the high cooling rates produced smaller and more globular grain structures. The highest cooling rate condition produced smaller and globular microstructure formation at 944 μm^2 and a circularity of 0.61, respectively. Meanwhile, the slow cooling condition produced the largest grain size at 1668 μm^2 and a circularity of 0.46. The results show that higher cooling rates result in a smaller and more spherical grain structure than other cooling conditions. This underlines the significant influence of the cooling rate on the development of the microstructure during the solidification process. This comprehensive thermal analysis study has shed light on the significant influence of Mg addition and different cooling conditions on the Al-Si alloy's thermal properties and microstructure formation. The results contribute to understanding alloy solidification and may have practical implications for materials engineering and manufacturing.

Keywords: Aluminium alloy; globular microstructure; grain refinement; semi-solid processing; thermal analysis

1. Introduction

The versatile and skilful utilisation of aluminium alloy across the various manufacturing sectors, such as packaging, medical equipment, electrical components, and automotive production, has undoubtedly led to considerable global economic growth. Nevertheless, intensive research is underway to exploit the potential of aluminium used in various manufacturing sectors. The needs for improved structural efficiency in the automotive and aerospace industries has led to the development of lighter, sturdier, and stronger materials, which are becoming increasingly important [1-3]. This is because using lighter and stronger materials can help reduce the structure's weight, thereby improving fuel efficiency and performance. Aluminium and its alloys play a vital role in the most used materials in mechanical design and the automotive industry. Aluminium alloy is widely recognised across multiple sectors for its exceptional qualities, including corrosion resistance, lightweight construction, high strength, remarkable resistance to low temperatures, and simplicity of extrusion moulding. The widespread use of aluminium alloys in casting industries is attributable to their distinctive corrosion resistance and malleability. Mg is the main alloying element in these alloy series, with the precipitation of Mg_2Si during solidification making the alloys heat-treatable [4].

Metal casting plays a crucial role in the manufacturing industry since it is heavily relied upon for the large scale production of a wide range of components. The manufacturing industry is currently confronting the crucial challenge of meeting demand and supply by producing materials of superior quality. However, the conventional casting technique has several drawbacks, such as porosity, hot ripping, and gas inclusions in the material [5-8]. In 1970, Flemings and Spencer discovered semisolid metal (SSM) processing at the Massachusetts Institute of Technology [9-11]. It was discovered that the viscosity of the Sn-15wt.%Pb alloy decreased as a result of applying shear force to the molten metal while it was solidifying. The SSM processing in the casting process can eliminate defects that occur in the standard casting process. Additionally, it has been observed that SSM processing results in materials with superior mechanical qualities and reduced porosity content. SSM processing has been shown to produce materials with enhanced mechanical properties and decreased porosity levels. The utilisation of this approach has gained extensive recognition as a casting process for manufacturing high-quality Mg and aluminium alloy products. The SSM processing produces a microstructure that is not dendritic or globular in type, which differs from the production of dendritic microstructures [9].

In early 1949, Cibula et al. discovered the grain refinement technique, which involves the use of titanium together with boron or carbon to effectively modify the particle size distribution within the alloy [12]. Subsequently, the technique of grain refinement, particularly the incorporation of titanium together with boron or carbon, has successfully produced a favourable refining impact on aluminium, enhancing the material's mechanical characteristics and surface quality. Grain refining has emerged as a preferred technique for creating superior characteristics and spherical grain structures required for semisolid metal (SSM) processing. Grain refining is a method that reduces casting errors by controlling the growth of grains during solidification, resulting in materials with smaller grain sizes. The primary goal of the grain refinement process is to enhance the mechanical properties of the alloy, precisely its strength, hardness, and ductility [13-14]. Cast components with refined grain structure are less prone to flaws such as

hot cracking and the formation of isolated areas with high porosity during the solidification process. Additionally, a refined grain structure enhances the pressure-tightness of the components [15].

The small and globular particle sizes in the as-cast state can improve the efficiency of various processes by reducing homogenization time, optimising the uniformity of recrystallized crystal structures, and enhancing the mechanical properties of the materials. The literature indicates that the alloys containing 1.0 and 1.5 wt.% Mg produced a more globular microstructure formation and a significant refinement of the grain structure [16-18]. The alloy's tensile strength was enhanced by adding 1.0 and 1.5 wt.% of Mg. The increased Mg content resulted in a reduction in particle size, an increase in the globular microstructure, and an enhancement of the alloy's mechanical properties. Nevertheless, due to the high amount of Mg addition, the percentage of elongation decreased. In summary, the addition of Mg influences the development of the grain structure and mechanical properties of aluminium alloys.

Microstructure and chemical element measurements were typically used to evaluate the quality of the materials [19-20]. The solidification process of Al-Si alloy involves several distinct phases, including nucleation, followed by the development of equiaxed dendrites that converge at the dendrite coherence point (DCP), the growth of secondary dendrite arms, and eutectic precipitation. The estimation of microstructure refinement is usually achieved by using secondary dendrite arm spacing (SDAS), which serves as a general indicator of the size of α-Al dendrites [21-23]. Thermal analysis is a method to analyse the characteristics of materials at various temperature conditions. Thermal analysis is an adequate and essential method for determining the physical properties of a sample as a function of temperature (T) versus time (t) while heating and cooling the sample according to a predetermined program [23]. The thermal analysis method was used to evaluate the discrepancies within the sample regarding chemical and physical characteristics. Additionally, thermal analysis is a crucial and alternative technique that enables the assessment of a melt's quality using phase change temperature and fraction solid temperature [25-26]. Thermal analysis provided the solidification latent heat information, such as the alloy's liquidus, solidus, and eutectic temperature during the solidification process. In addition, the thermal analysis also provided information on the fraction solid and dendritic coherency point (DCP) that significantly affect the alloy's flowability. Differential thermal analysis (DTA) and differential scanning calorimetry (DSC) are among the techniques used in the thermal analysis method [1, 25, 27-28]. The DTA concept was based on measuring the temperature variations in the sample. In contrast, DSC measures the energy differences directly rather than the temperature changes at low heating rates to avoid sensitivity losses [1, 27, 29].

Nevertheless, these procedures are expensive due to the high cost of the equipment, and they cannot precisely characterise the required parameter [1, 30]. However, an alternative thermal analysis, known as cooling curve analysis (CCA), was developed to obtain the molten metal data before casting. This method used the concept of measuring the heat change within the melt using two thermocouples developed by Bäckerud [26]. Computer-aided cooling curve analysis (CA-CCA), one of the methods used in thermal analysis, is the most straightforward and practical to use in a laboratory environment. Thermal and microstructural analyses are two methods used to control and characterise molten alloys. Previous research has shown that the cooling rate significantly influences microstructure development, with higher cooling rates leading to a finer microstructure and enhanced mechanical properties [25, 31, 32]. Furthermore, higher cooling rates led to finer particles in the primary phase [31]. Thus, these research objectives are to determine

the effect of 1 wt.% Mg addition on the solidification characteristics of aluminium alloy cooling rate using the CCA method before semisolid metal processing.

2. Experimental procedure

The chemical composition of the as-received material was analysed using Foundry Master Uv spectroscopy. The chemical composition test was repeated thrice, and the average result was presented in Table *1*.

Table 1 Chemical composition of Al-Si alloy.

Element	Si	Zn	Cu	Fe	Ni	Mn	Mg	Cr	Ti	Al
Composition (wt.%)	9.76	1.48	1.16	0.69	0.54	0.31	0.23	0.11	0.09	Balance

A mass of 200 g of the as-received material was cut and labelled A, B, C, and D, respectively. The materials were then put into 2 kg graphite with the addition of 1 wt.% of pure Mg. Figure *1* represents the dimensions of the graphite crucible used during the melting and solidification processes. The crucible was melted in an electric furnace at a frequency of 60 Hz and 220 V until the temperature reached 800 °C. As soon as the samples began to melt, the heating process was maintained for five minutes to homogenize the molten alloy. Then, the melt was stirred for 10 s to ensure the alloy and Mg were well mixed. The crucible was taken out of the furnace and allowed to cool to room temperature. This condition is known as the normal cooling condition (A). Meanwhile, the slow cooling condition (B) was achieved when the crucible was allowed to cool within the Kaowool insulator chamber. In addition, the fast (C) and fastest (D) cooling conditions were attained when the forced airflow was directed at the crucible at minimum and maximum speed, respectively. A pair of K-type thermocouples with a diameter of 1 mm were connected with the data acquisition device Ni 9129 to measure the melt's temperature difference. Data acquisition device Ni 9129 is able to read 25 samples per second at a frequency of 5 Hz. The thermocouple was immersed at the centre of the crucible, and the other one was immersed near the wall. Both of the thermocouples` tips are immersed 85 mm apart from the top surface of the crucible, and the gap between the two thermocouples is about 15 mm. The experimental setup for thermal analysis is shown in Figure 2.

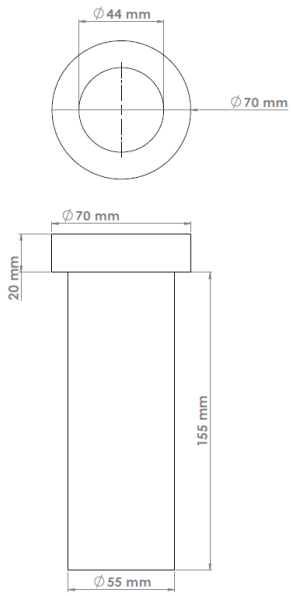

Figure 1: Dimension of the graphite crucible used in this experimental work.

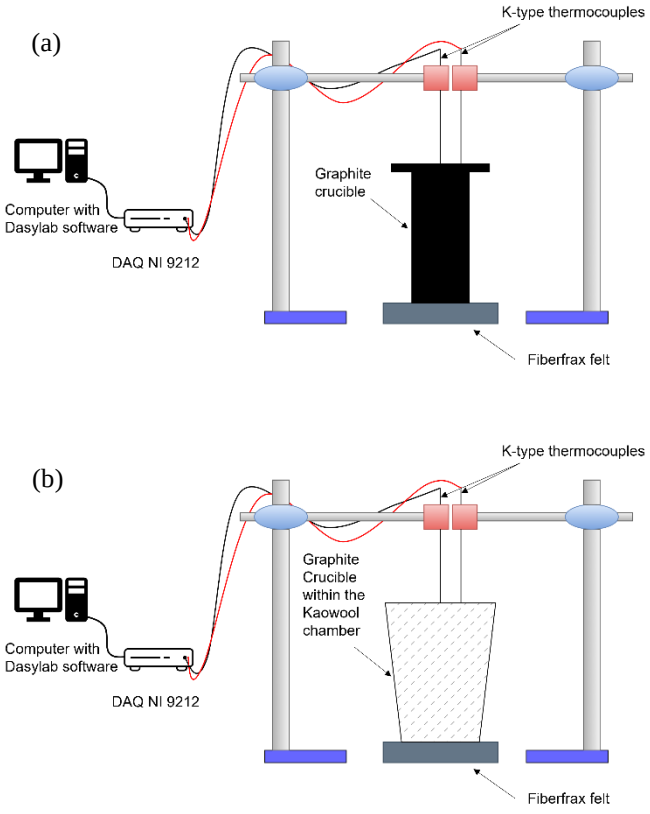

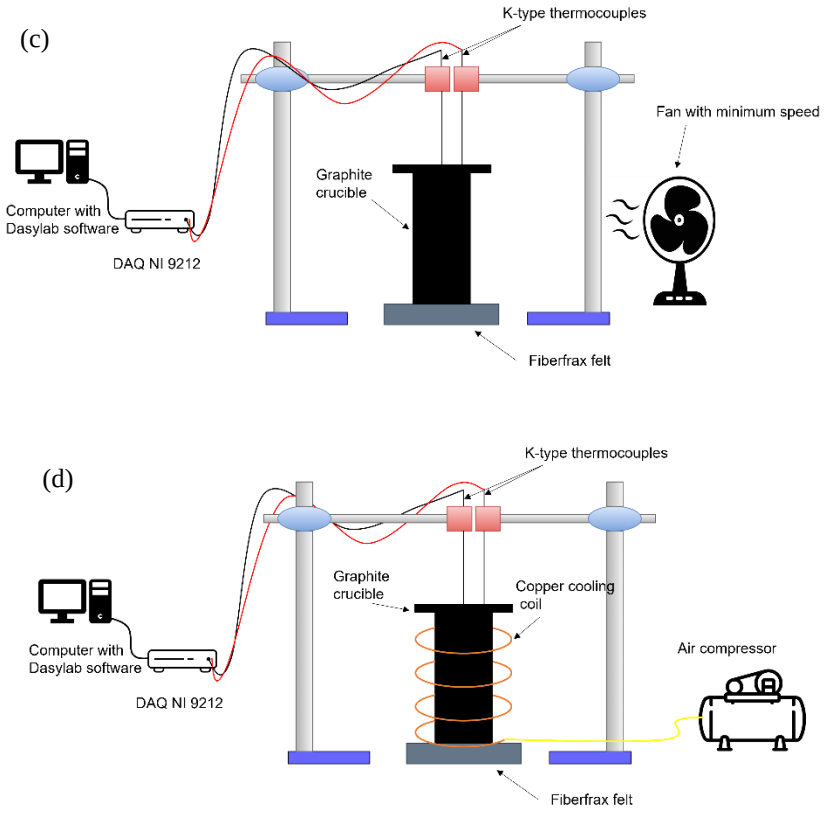

Figure 2: Thermal analysis experimental setup for (a) normal cooling, (b) slow cooling, (c) fast cooling and (d) fastest cooling conditions.

The NI 9219 data acquisition device captured the data once the cooling process began, and it was subsequently transmitted to the user's PC. The experiment was repeated three times for each cooling rate condition to obtain the average value. OriginPro 2019b was used to perform data analysis and plot the cooling curve alongside the first derivative curve. A baseline was then established using the first derivative curve. It represents the rate of cooling that could have occurred without latent heat. The trend line is identical to the first derivative curve in the single-phase regions above the liquidus temperature and below the solidus temperature. In the single-phase zones, which are above the liquidus temperature and below the solidus temperature, it exhibits the same trend line as the first derivative curve [1-2]. The solid fraction was computed using the accumulative area between the first derivative and the baseline based on Equation 1. The first derivative curve was denoted by FDC while the baseline curve is delineated by DBL. The t_e and t_s was defined by end time of solidification and the beginning of solidification. The determination of the dendritic coherence point (DCP) used either the largest temperature difference or the first minimum point on the temperature difference curve during the solidification duration.

$$f_s = \frac{\int_{ts}^{t} FDC-DBL}{\int_{ts}^{te} FDC-DBL} = \frac{\text{Cumulative area till instant of time}}{\text{Total area}} \quad (1)$$

Where cooling curve (CC) and baseline (BL). The cooling rate was calculated at the temperature difference between the initial temperature points, $T_{o,}$ and the point 50 °C after the liquidus temperature of the alloy,

$$Cooling\ rate = \frac{T_0 - T_{liq+50\,℃}}{t_0 - t_{liq+50\,℃}} \quad (2)$$

The microscopic sample was sectioned 20 mm from the bottom of the crucible, and the centre region was mounted using Bakelite resin with a pressure of 60 bars, a heating time of 2 minutes, and a cooling time of 3 minutes. Then, the samples were ground using a grinding machine with 120, 320, 400, 600, 1200, and 2400 grit-size silicon carbide. The grinding speed was set at 200 rpm to reduce the cutting damage on the sample surface. Next, the samples were polished using 6, 3, and 1-micron diamond suspension for 10 minutes with a polishing speed of 150 rpm. Then, the samples were polished using colloidal silica suspension before being etched using Keller's reagent for 5 s. The microscopic images of the structure were captured using an optical microscope and the Motic Image Plus 3.0 software. A selection of slow and normal cooling settings was conducted to study the composition and identify the phase. The microstructures of the materials were analysed using an Olympus optical microscope (OM), while the different phases present in the samples were detected through the utilization of a Jeol JSM-IT 200 scanning electron microscope (SEM) equipped with energy dispersive X-ray spectroscopy (EDX). Furthermore, X-ray diffraction (XRD) analysis was performed using the PANalytical X'Pert³ Powder instrument. In addition, the analysis was performed using the Image-J software program to determine the grain size, circularity, and feret diameter of the a-Al phase in the samples. The circularity can be calculated using equation 3.

$$Circularity = 4\pi\ x\ area/Perimeter^2 \quad (3)$$

3. Results and Discussion

I. Thermal Analysis

Figure *3* depicts the cooling curve, first derivative curve, solid fraction, and DCP curve recorded for the normal cooling condition. Figure *3* (a) shows the cooling curve of the normal cooling condition during the solidification process. Due to heat convection from the wall surface to the ambient, the wall temperature is slightly lower than the temperature at the centre of the crucible, as shown in the figure. The cooling rate was measured at the temperature between the initial point, 630 °C, and 50 °C before the liquidus temperature, as depicted by Equation 2, within the specified time. The cooling rate determined by the slope of the cooling curve above the liquidus region was at 1.22 °C/s. The thermal characteristics, such as solidus, liquidus, and eutectic temperature, of the molten alloy can be obtained by performing further analysis on the cooling curve by acquiring the first derivative. The cooling curve,

also known as the derivative curve, facilitates the identification of phase changes that occur in the alloy during solidification. Previous research provided a clear explanation of the nucleation identification process, crystal development, and phase transitions of the alloy during the solidification phase in the temperature profile [2, 33]. Figure *3* (b) shows that for the normal cooling rate condition, the liquidus, solidus, and eutectic temperatures were found at 571 °C, 459 °C, and 480 °C, respectively. In the meantime, Figure *3* (c) represents the solid fraction graph calculated between the liquidus and solidus temperatures of the molten alloy. The solid fraction during solidification is very crucial to determining the processing parameters for semisolid metal processing, including the pouring temperature and holding time [1]. In Figure *3* (d), the DCP for normal cooling conditions occurred at 94.7 s, corresponding to temperatures of 563 °C, respectively.

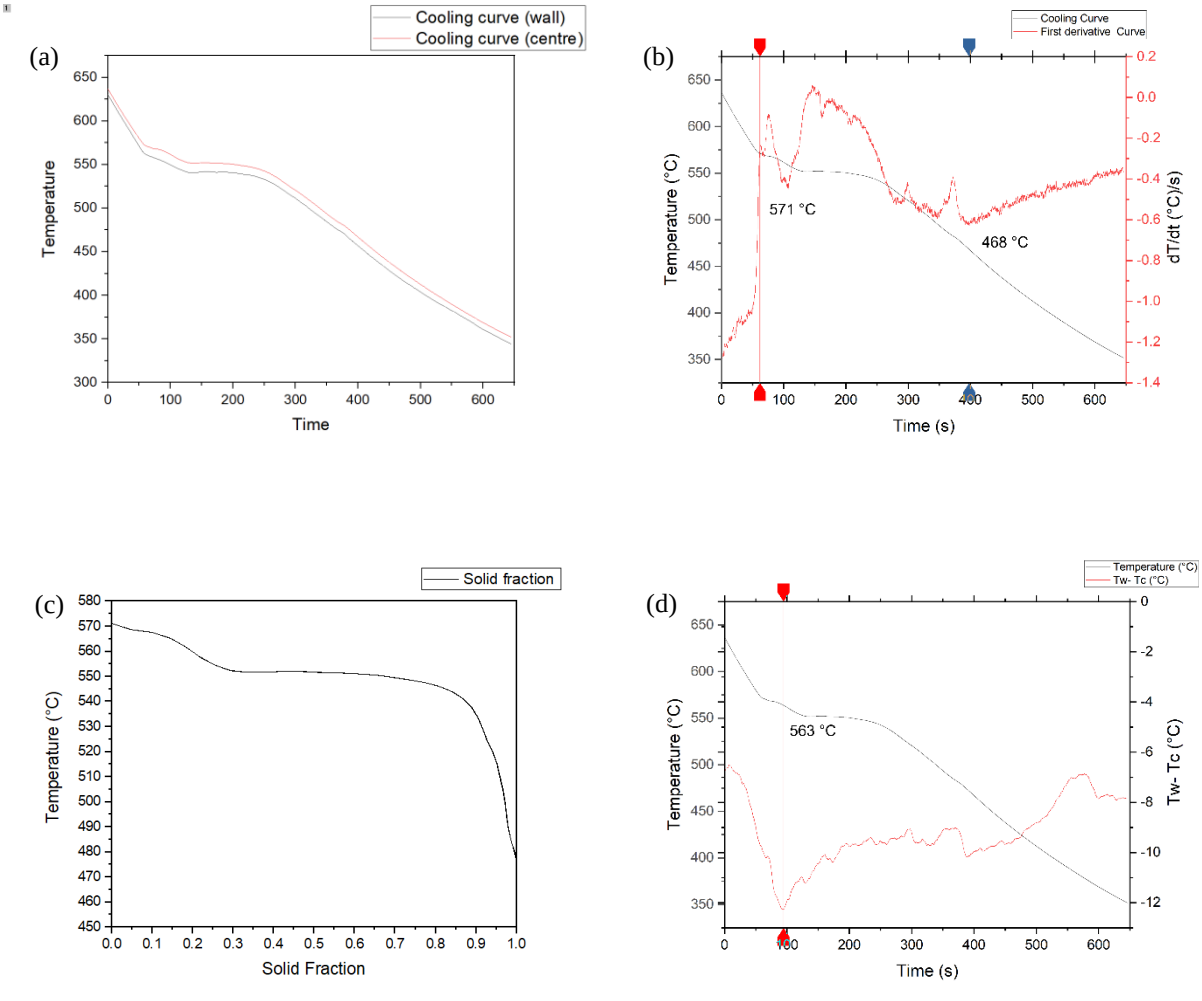

Figure 3: Normal cooling condition with a cooling rate of 1.22 °C/s with (a) cooling curve, (b) cooling curve and first derivative curve, (c) fraction solid curve, and (d) DCP curve.

The thermal profile for slow cooling conditions are shown in Figure *4*. Figure *4*(a) shows the cooling curve between the wall and centre temperature during the solidification process. From the cooling curve graph, the cooling rate calculated was 0.17 °C/s beyond the liquidus temperature. Based on the cooling curve in Figure *4*(b), the liquidus,

solidus, and eutectic temperatures were found at 579 °C, 464 °C, and 479 °C, respectively. The calculated fraction of solids for slow cooling conditions is shown in Figure *4*(c). The DCP for the slow cooling curve occurred at time 861.1s, corresponding to temperatures of 567 °C respectively.

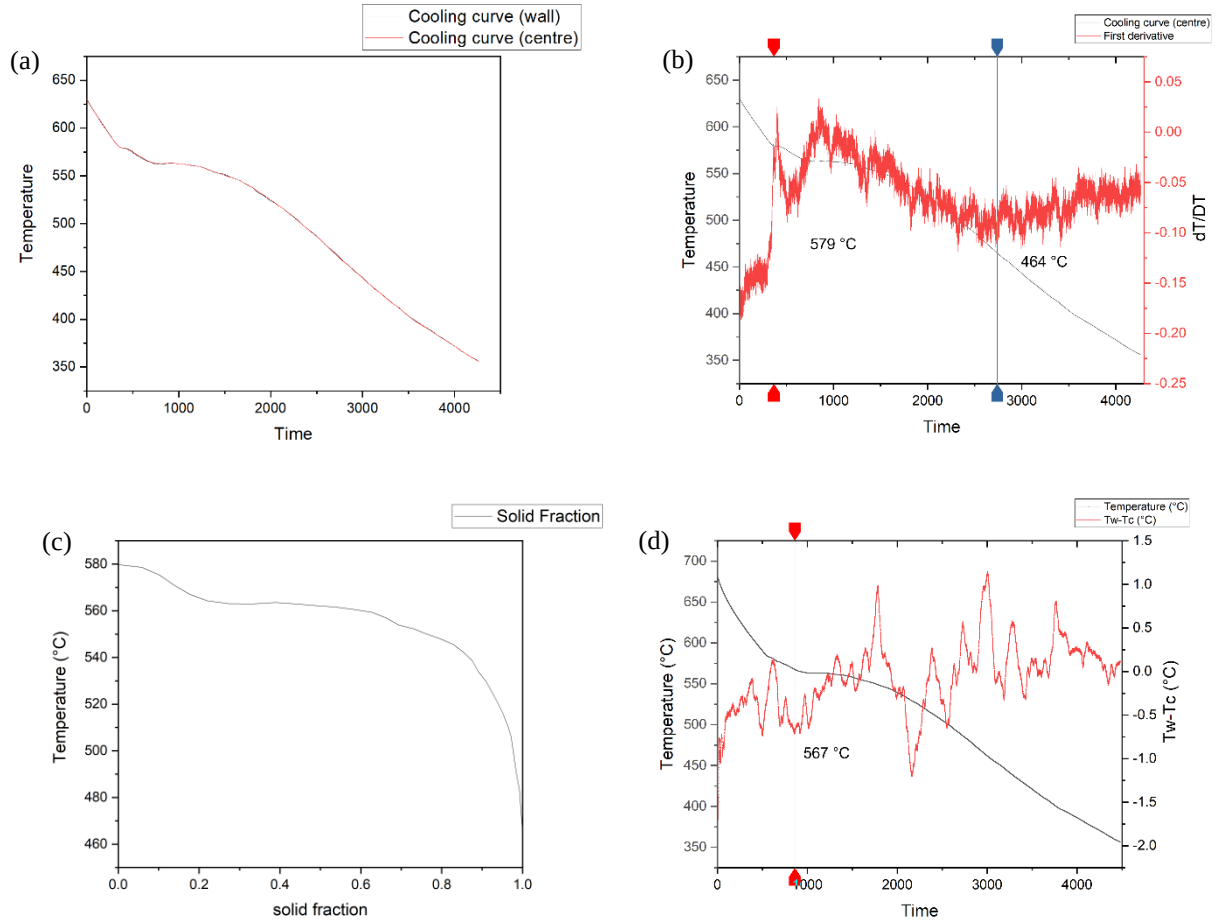

Figure 4: Slow cooling condition with cooling rate of 0.17 °C/s with (a) cooling curve, (b) cooling curve and first derivative curve, (c) fraction solid curve and (d) DCP curve.

Figure *5* shows the cooling curve for fast cooling rate conditions. The cooling rate for the fast cooling rate in Figure *5* (a) was determined to be 1.58 °C/s based on the cooling curve slope beyond the liquidus temperature. Based on Figure *5*(b), the liquidus, solidus, and eutectic temperatures were found at 577 °C, 477 °C, and 503 °C. In contrast, the corresponding calculated fraction of solid temperature is presented in Figure *5* (c). The DCP for the fast cooling curve occurred at time 80.6s, corresponding to temperatures of 567 °C, respectively. Figure *6* (a) presents the cooling curve for the fastest cooling condition. The cooling rate for the fastest cooling condition was determined to be 5.66 °C/s based on the cooling curve slope beyond the liquidus temperature. Figure *6* (b) shows that the liquidus, solidus, and eutectic temperatures were found at 571 °C, 459 °C, and 480 °C. The relationship between temperature and fraction solids is presented in Figure *6* (c). The DCP for the fastest cooling curve occurred at time 48.5s, corresponding to temperatures of 542 °C, respectively. In this particular experimental study, it was observed that the phase transition temperatures for the alloy could be varied by manipulating the cooling rate. Determining solidification

parameters, especially liquidus and solidus temperature, is of utmost importance as it serves as a crucial reference temperature for processing SSM raw material billets [34-35]. Table *2* shows the solidification characteristics of the alloy under various cooling conditions.

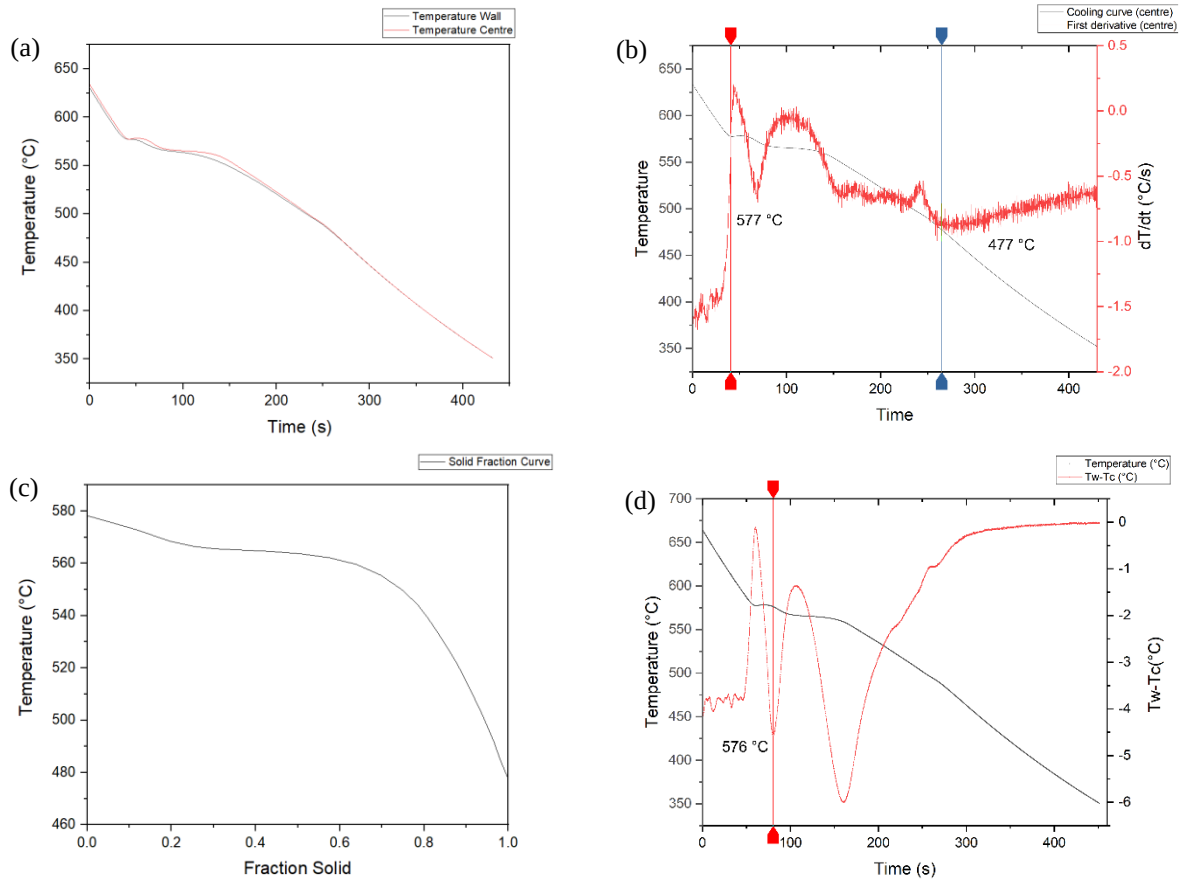

Figure 5: Fast cooling condition with cooling rate of 1.58 °C/s with (a) cooling curve, (b) cooling curve and first derivative curve, (c) fraction solid curve and (d) DCP curve.

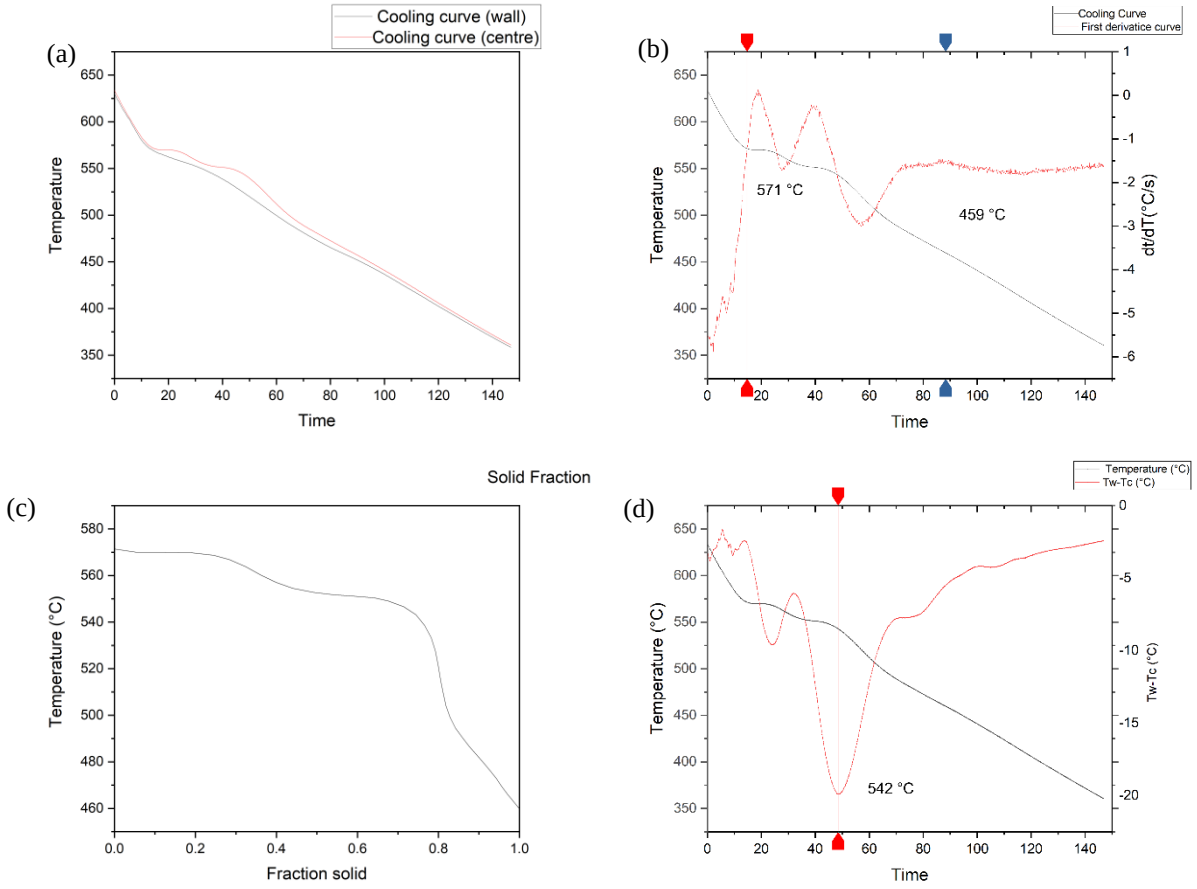

Figure 6: Fastest cooling condition with cooling rate of 5.66 °C/s with (a) cooling curve, (b) cooling curve and first derivative curve, (c) fraction solid curve and (d) DCP curve.

Table 2: solidification characteristic of the Al-Si alloy with Mg addition under various cooling conditions.

Cooling rate (°C/s)	Liquidus Temperature (°C)	Solidus Temperature (°C)	Eutectic Temperature (°C)	DCP (°C)
0.17	579	464	479	567
1.22	571	496	468	563
1.58	577	481	503	576
5.66	571	459	466	542

II. Microstructure Analysis

The relationship between cooling rate and secondary dendrite arm spacing (SDAS) is presented in *Table 3*. The lowest cooling rate, which is 0.17 °C/s, produces the largest SDAS values, which are 54.8 µm compared to other cooling conditions. Meanwhile, the fast-cooling condition with a cooling rate of 5.66 °C/s has the lowest SDAS value at 18.9 µm. Increasing the cooling rate from 0.17 to 5.66 °C/s changed the SDAS from 54.8 to 18.9 µm. This experimental work's findings correlate with the literature, where the higher cooling rate will produce a smaller SDAS value [20].

Table 3: Relationship between cooling rate and SDAS.

Cooling rate (°C/s)	Average SDAS (µm)
0.17	54.8 ± 5.6
1.22	46.8 ± 4.3
1.58	34.3 ± 3.4
5.66	18.9 ± 2.2

The effect of different cooling rates on the microstructure formation within the samples was analysed using qualitative methods. Figure *7* depicts the microstructure formation under different cooling rate conditions. After the solidification was completed, the samples for analysis were analysed in the centre of the crucible. There was an obvious difference between the microstructure formations in Figure *7*. The difference in microstructure formation was due to the difference in the cooling rate applied during the solidification process.

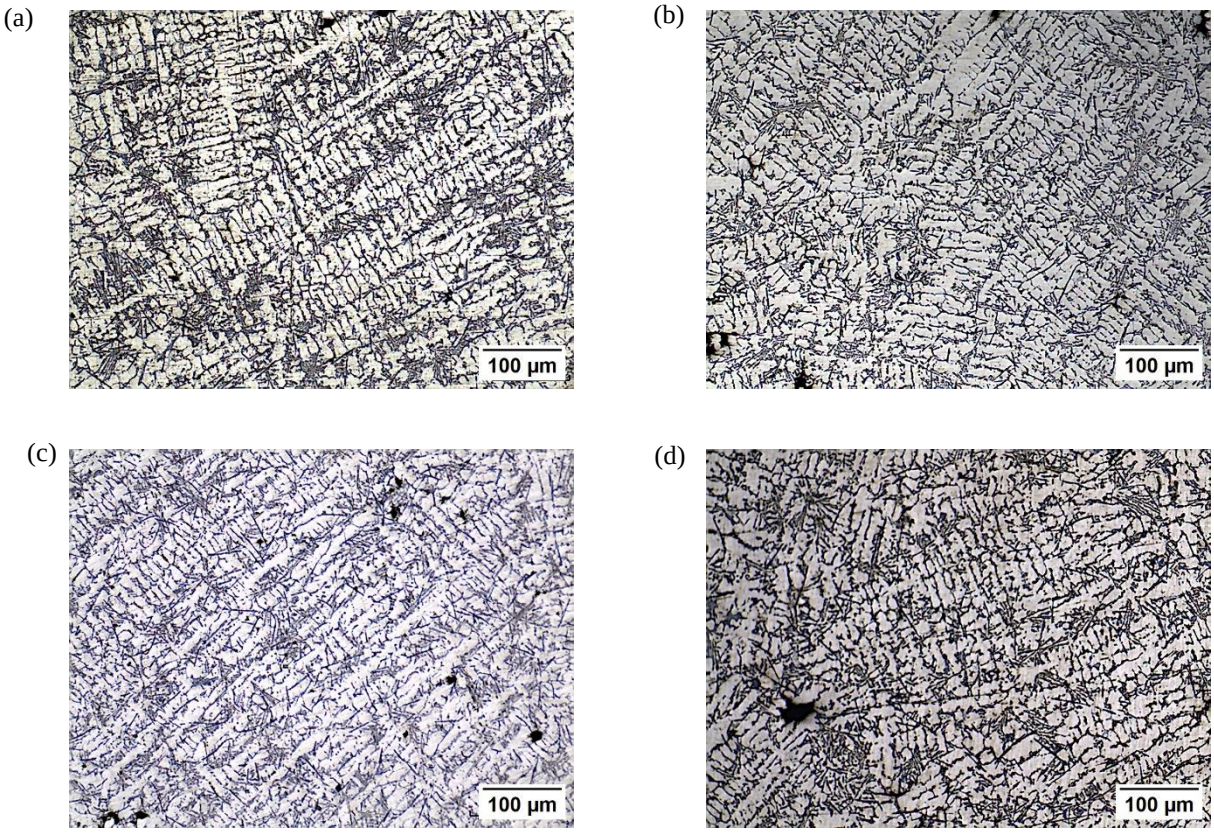

Figure 7: The microstructure formation with 5x magnification for (a) normal cooling condition (1.22°C/s), (b) slow cooling condition (0.17°C/s), (c) fast cooling condition (1.58°C/s) and (d) fastest cooling condition (5.66°C/s).

The grain size, circularity, and ferret diameter were measured for each cooling condition to determine the effect of different cooling rates on each microstructure formation. Figure *8* represents the result of the grain size measurement of each microstructure formation for each cooling condition. The findings indicate that a fine and globular grain structure has evolved as a result of the increased cooling rate. The fastest cooling rate condition of 5.66 °C/s has the smallest grain size, which was 944 μm^2 and has the most globular grain structure with a circularity

of 0.63 compared to other cooling rate conditions. The grain size for normal (1.22 °C/s) and fast (1.58 °C/s) cooling conditions was measured at 1205 µm^2 and 1037 µm^2 respectively. Meanwhile, the grain size for slow cooling conditions of 0.17 °C/s has the largest grain size with 1668 µm^2 and circularity of 0.46.

The results clearly differentiate between the higher cooling rates producing smaller grain sizes, which is in agreement with the literature review on the earlier study on the impact of cooling rates on the microstructure of aluminium alloys [1, 28, 32, 36-37]. Table *4* summarises the effect of cooling rate conditions on microstructure formation during the solidification process. The increase in cooling rate increases the heat removal from the molten alloy. Thus, the molten alloy is cooled to a temperature beyond the equilibrium melting point. Consequently, nuclei formation is facilitated by the existing suitable undercooling [1, 36]. As the cooling rate and undercooling increase, the critical nucleus size decreases, leading to changes in the embryo's nuclei [37]. Moreover, the solidification time decreases as the cooling rate and the solidification temperature range increase. The nuclei's development is inhibited as the time to solidify the melt is shorter. Hence, the fastest cooling rate produces a smaller grain size than other cooling conditions.

Table 4: Summary of the effect of cooling rate on the microstructure formation during the solidification process.

Cooling rate (°C/s)	Grain Size (µm^2)	Circularity	Feret Diameter (µm)
0.17	1668	0.46	77
1.22	1205	0.57	62
1.58	1037	0.59	53
5.66	944	0.61	48

(a)

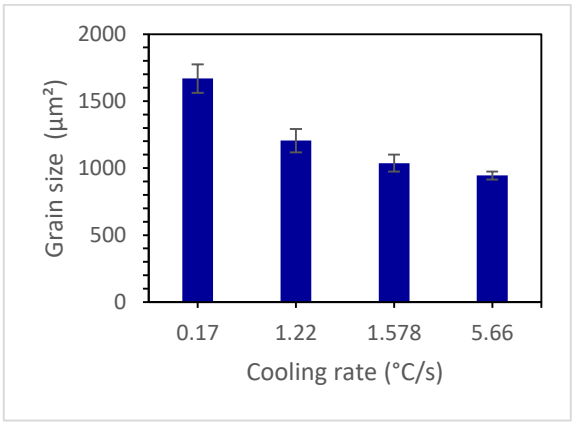

(b)

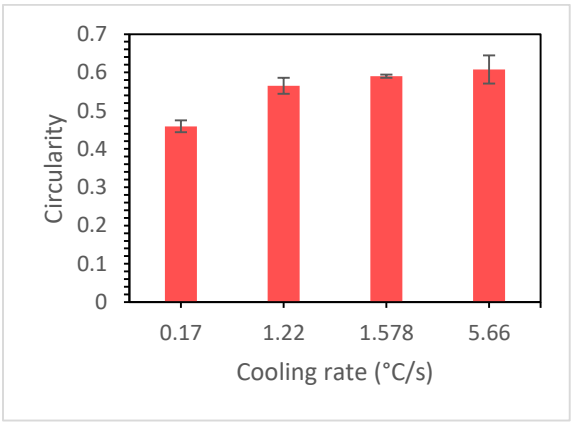

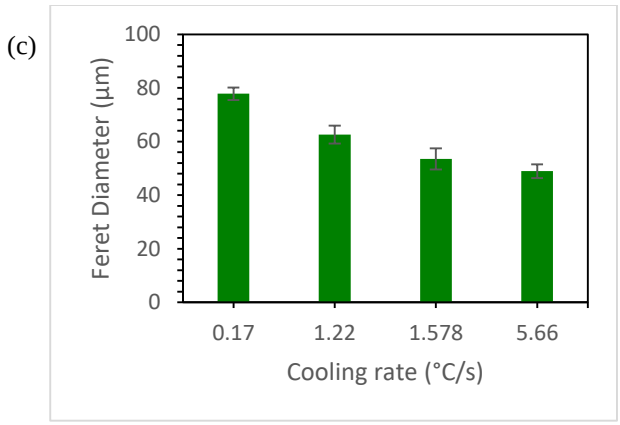

Figure 8: Grain size measurement for different cooling conditions with (a) average grain size, (b) circularity and (c) ferret diameter.

III. SEM, EDX Analysis and XRD Analysis

Figure *9* depicts SEM microscopic images and EDX spectra revealing intermetallic phases under normal cooling conditions. The eutectic Al-Si phase conspicuously surrounds the primary (Al) phase in the microstructure. Figure *9* shows the selected area and the chemical composition of the sample under normal cooling conditions. Al, Si, Cu, and Mg were determined to be the four primary elements produced during normal cooling.

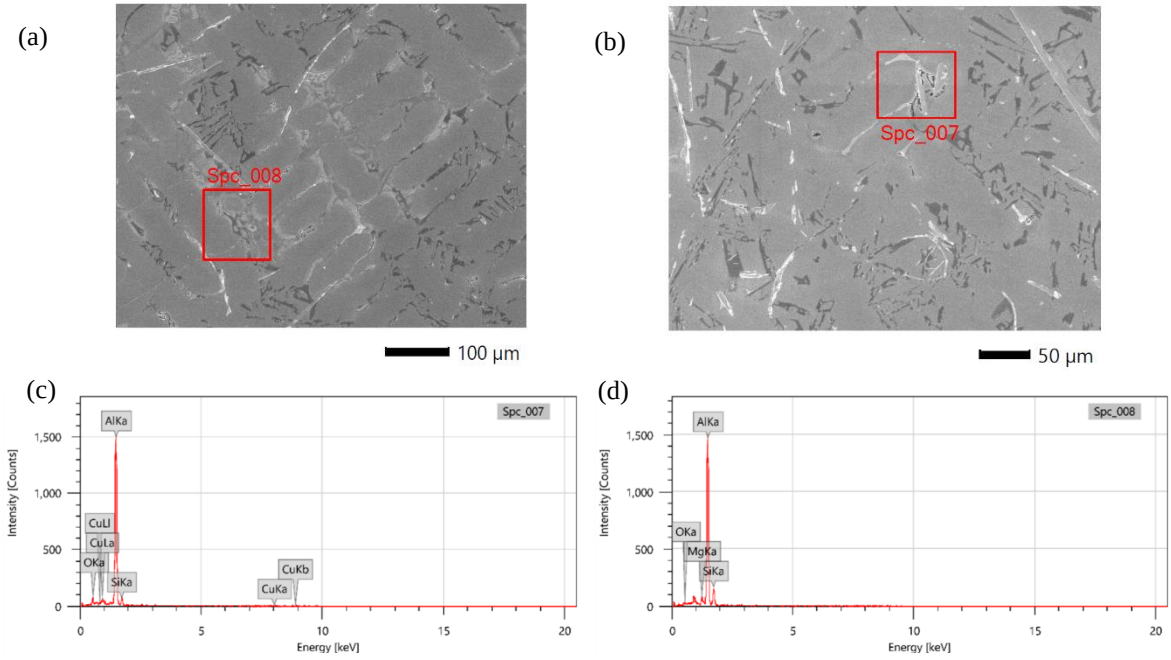

Figure 9: The microscopic images with (a & b) SEM images and (c & d) EDX analysis of normal cooling conditions.

Figure *10* illustrates the spectrum of the quantitative EDXS analysis of the phases identified in the indicated region. Five significant elements were detected in the sample, including Al, Mg, Si, Cu, and Fe. A trace of iron (Fe) was detected in a slow cooling rate sample, while this element was not previously detected in a sample cooled under normal conditions.

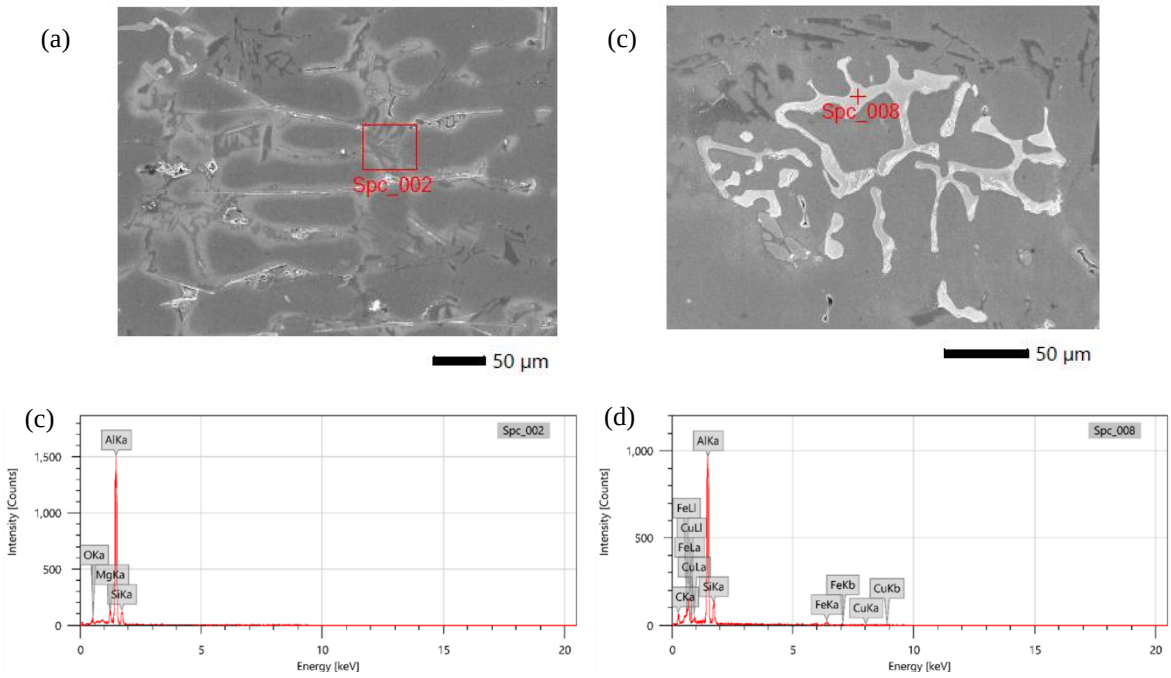

Figure 10: The microscopic images with (a & b) SEM images and (c & d) EDX analysis of slow cooling conditions.

Figure *11* (a) shows the X-ray diffraction spectra of the alloy at normal cooling conditions. There are several peaks composed of the peaks of the elements Al and Si. The distinct peak for the Al and Si elements was detected at several locations, which are at 28.71°, 38.73°, 47.58°, 65.31°, and 78.50°, respectively. The microstructure phases at normal cooling consist of α-Al, eutectic Si, and Zn. Meanwhile, the intermetallic compounds consist of $Cu_{0.7}Zn_2$, $Al_{35}Cu_{47}$ and $AlCu_3$. The X-ray diffraction spectra of the alloy during slow cooling are shown in Figure *11* (b). There are several peaks of the Al and Si elements found at different locations, which are at 28.37°, 38.42°, 47.24°, 56.06°, 64.99°, 76.35°, 78.15°, and 88.03°. Figure 11 (b) shows that the microstructure phase consists of α-Al, Si and Cu, while the intermetallic compounds consist of Al_2Cu and $Al_4Cu_2Mg_8Si_7$, respectively.

The eutectic composition of the alloys consisted of silicon (Si), aluminium, copper (Al2Cu), and other particles dispersed in an aluminium matrix (Al). The morphology of these constituents exhibited irregular shapes characteristic of a typical eutectic microstructure. The examination carried out with EDX shows the presence of traces of silicon (Si), copper (Cu), and magnesium (Mg) in the aluminium matrix. The eutectic phase experienced a significant accumulation of these components near the grain boundaries. It was discovered that the addition of Mg elements precipitated the intermetallic phases of $Al_4Cu_2Mg_8Si_7$ by consuming some of the Al_2Cu and eutectic Si [18, 39].

It has been shown that the observed high cooling rate is influenced by the presence of Mg, which modifies the

eutectic Si structure [39]. In their study, Aguilera et al. [39] found that a more favourable degree of modification of the eutectic silicon structure was achieved when the cooling rate reached 4 °C/s. The eutectic structure of the silicon changed when the Mg concentration was increased from 0.4 to 0.6 wt.%. The resulting morphology had a more fibrous structure, characterised by a limited occurrence of acicular and laminar particles. In contrast, the formation of a fibrous structure with a limited number of acicular and laminar particles is not possible at cooling rates below 2 °C/s. Increasing the cooling rate led to a noticeable reduction in the size of the silicon particles, accompanied by a more uniform distribution in the microstructure. Despite the reduction in size of the silicon particles, their structure exhibited a persistent acicular nature, albeit with fragmentation. When the cooling rate increases, the temperature drops so rapidly that the high-temperature excretions do not have enough time to form [40]. The uneven morphology of the second phase in this model alloy is commonly attributed to variations in the temperature gradient, the degree of supercooling, and the changes in composition that occur during the solidification process. The microstructural morphology of an alloy is influenced by the rate of cooling during the solidification phase. This cooling rate plays a crucial role in determining the size and shape of the secondary phase of the alloy [41]. When the cooling rate is increased, the magnitude of the energy fluctuations increases accordingly, leading to an acceleration of nucleation. The phase transitions between liquid and solid occur prior to the growth of the crystal grain, which leads to the formation of smaller grains and a deviation from the state of equilibrium.

(a)

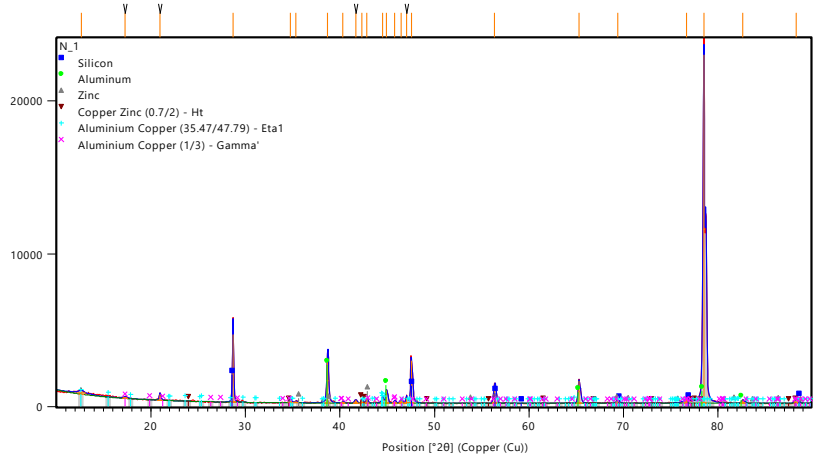

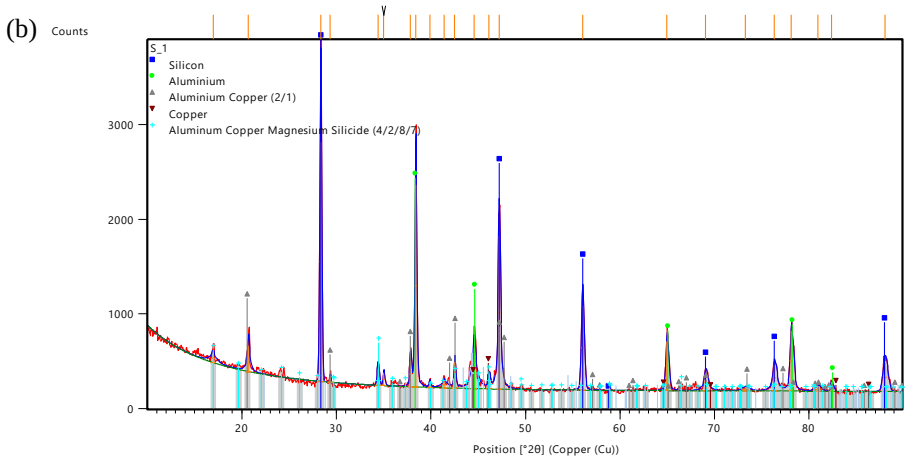

Figure 11: The XRD spectra for (a) normal cooling condition and (b) slow cooling condition.

4. Conclusion

In this experimental work, the addition of Mg to the Al-Si alloy results in an improvement in the solidification characteristics and microstructure formation. According to the results of the experimental work above, the following conclusion may be drawn:

1. The different cooling rate conditions influence the thermal properties of the alloy during the solidification process. The thermal analysis experiment is crucial to determine the thermal profile of the alloy and develop parameters for semisolid metal processing.
2. The cooling rate significantly affects secondary dendrite arm spacing (SDAS). Increasing the cooling rate from 0.17 to 5.66°C/s changes the SDAS value from 54.8 to 18.9 µm.
3. The cooling rate influenced the development of the grain structure during the solidification process. The low cooling rate at 0.17°C/s produces largest grain size at 1668 μm^2 with the circularity and ferret diameter at 0.46 and 77 µm, respectively. Meanwhile, the fastest cooling rate, 5.66 °C/s, produced the smallest grain size compared to other cooling rates at 944 μm^2. In addition, the circularity and ferret diameter for the fastest cooling rate at 0.61 and 48 µm, respectively.
4. The X-ray diffraction spectra analysis for normal cooling conditions shows that intermetallic components' formation consists of $Cu_{0.7}Zn_2$, $Al_{35}Cu_{47}$, and $AlCu_3$. Meanwhile, the X-ray diffraction spectra for slow cooling conditions consist of intermetallic components such as Al_2Cu and $Al_4Cu_2Mg_8Si_7$.

Acknowledgements

The authors would like to thank Universiti Malaysia Pahang Al-Sultan Abdullah for laboratory facilities and financial support under grant number RDU210366.

Author contribution: The manuscript was written by Muhammad Faez Bin Mohamad Tajudin. The manuscript was supervised by Dr Asnul Hadi Bin Ahmad, Dr Juliawati Binti Alias, Mrs Nur Azhani Binti Abd Razak, and Dr Sumsun Naher.

Funding: Universiti Malaysia Pahang Al-Sultan Abdullah and Centre for Automotive Engineering for laboratory facilities and providing financial support under the Internal Research Grant of RDU210366.

Availability of data and material: Data can be made available upon request, subject to the approval of all parties involved in the research.

Ethics approval and consent to participate: The manuscript has not been submitted to any other journal for simultaneous consideration.

Consent for publication: The participants provided informed consent for the publication of their statements. All authors voluntarily agree to participate in this research study.

Competing interest: On behalf of all authors, the corresponding author states that there is no conflict of interest.

References

[1] N. A. Razak, A. H. Ahmad, And M. M. Rashidi, "Thermal Profile and Microstructure of Wrought Aluminium 7075 For Semisolid Metal Processing," International Journal of Automotive and Mechanical Engineering, Vol. 17, No. 2, Pp. 7842–7850, Apr. 2020, Doi: 10.15282/Ijame.17.2.2020.03.0584.

[2] Ma X. H. And Abd Razak, N. A. (2023). The Change of Solidification Parameters on Hypoeutectic Aluminum–Silicon Alloy Under Different Cooling Rates. In M. S. And K. S. And H. M. A. And S. M. S. Ismail Muhammad Yusri and Mohd Sani (Ed.), Technological Advancement in Mechanical and Automotive Engineering (Pp. 263–278). Springer Nature Singapore. Https://Doi.Org/10.1007/978-981-19-1457-7_21.

[3] P. Gasson, "Light Alloys: From Traditional Alloys to Nanocrystals – Fourth Edition I. Polmear Elsevier Butterworth-Heinemann, Linacre House, Jordan Hill, Oxford, Ox2 8dp, Uk. 2006. 421pp Illustrated. £49.99. Isbn 0-7506-6371-5.," The Aeronautical Journal, Vol. 110, Pp. 394–395, Jun. 2006, Doi: 10.1017/S000192400008670x.

[4] M. S. Salleh, A. A. Rahman, R. I. R. Abdullah, N. Siswanto, And S. Subramonian, "Effect of Different Mg Content on Microstructure and Mechanical Properties of Thixoformed Al-Si-Cu-Mg Alloys," Jurnal Tribologi, Vol. 32, Pp. 16–28, 2022.

[5] Liu, F., Zhu, X., & Ji, S. (2020). Effects Of Ni on The Microstructure, Hot Tear and Mechanical Properties of Al–Zn–Mg–Cu Alloys Under As-Cast Condition. Journal Of Alloys and Compounds, 821, 153458. Https://Doi.Org/Https://Doi.Org/10.1016/J.Jallcom.2019.153458.

[6] S. Chayong, H. V. Atkinson, And P. Kapranos, "Thixoforming 7075 Aluminium Alloys," Materials Science and Engineering A, Vol. 390, No. 1–2, Pp. 3–12, 2005, Doi: 10.1016/J.Msea.2004.05.004.

[7] M. Zhen Et Al., "Rheological Behaviour of Partially Solidified A356 Alloy: Experimental Study and Constitutive Modelling," J Alloys Compd, Vol. 803, May 2019, Doi: 10.1016/J.Jallcom.2019.06.345.

[8] M. A. M. Arif, M. Z. Omar, Z. Sajuri, And Assoc. Prof. Ir. Ts. Dr. M. Salleh, "Effects of Cu and Mg on Thixoformability and Mechanical Properties of Aluminium Alloy 2014," Transactions of Nonferrous Metals Society of China, Vol. 30, Pp. 275–287, May 2020, Doi: 10.1016/S1003-6326(20)65212-8.

[9] Spencer, D.B., Mehrabian, R. & Flemings, M.C. Rheological Behavior of Sn-15 Pct Pb in The Crystallization Range. Metall Trans 3, 1925–1932 (1972). Https://Doi.Org/10.1007/Bf02642580.

[10] A. H. Ahmad, S. Naher, And D. Brabazon, "The Effect of Direct Thermal Method, Temperature and Time on Microstructure of A Cast Aluminum Alloy," Materials And Manufacturing Processes, Vol. 29, No. 2, Pp. 134–139, 2014, Doi: 10.1080/10426914.2013.822980.

[11] M. F. M. Tajudin, A. H. Ahmad, And M. M. Rashidi, "Effects of Different Processing Parameters on The Semisolid Microstructure of Al6061 Produced by A Direct Thermal Method," Iop Conf Ser Mater Sci Eng, Vol. 1092, No. 1, P. 012008, 2021, Doi: 10.1088/1757-899x/1092/1/012008.

[12] A. I. O. Zaid, "Effect of Molybdenum Addition to Za22 Grain Refined by Ti+B On Its Metallurgical and Mechanical Characteristics," Int J Sci Eng Res, Vol. 7, No. 4, Pp. 591–595, 2016, Doi: 10.14299/Ijser.2016.04.006.

[13] Y. Gu, R. Huang, And Y. Hao, "Review on Grain Refinement of Metallic Materials to Regulate Cellular Behaviour," Metals, Vol. 12, No. 5. Mdpi, May 01, 2022. Doi: 10.3390/Met12050829.

[14] M. F. M. Tajudin, A. H. Ahmad, J. Alias, N. A. A. Razak, And N. A. Alang, "Grain Refinement in Semisolid Metal Processing: Current Status and Recent Development," International Journal of Advanced Manufacturing Technology, Vol. 124, No. 5–6. Springer Science and Business Media Deutschland Gmbh, Pp. 1379–1399, Jan. 01, 2023. Doi: 10.1007/S00170-022-10590-9.

[15] L. Bäckerud, G. Chai, And J. Tamminen, Solidification Characteristics of Aluminum Alloys: Foundry Alloys. In Solidification Characteristics of Aluminum Alloys. Skanaluminium, 1990. [Online]. Available: Https://Books.Google.Com.My/Books?Id=Majyaaaacaaj

[16] K. S. Alhawari, M. Z. Omar, M. J. Ghazali, M. S. Salleh, And M. N. Mohammed, "Dry Sliding Wear Behaviour of Thixoformed Hypoeutectic Al-Si-Cu Alloy with Different Amounts of Magnesium," In Composite Interfaces, Taylor And Francis Ltd., Jul. 2016, Pp. 519–531. Doi: 10.1080/09276440.2016.1164496.

[17] M. S. Salleh, M. Z. Omar, K. S. Alhawari, M. N. Mohammed, M. A. M. Ali, And E. Mohamad, "Microstructural Evolution and Mechanical Properties of Thixoformed A319 Alloys Containing Variable Amounts of Magnesium," Transactions of Nonferrous Metals Society Of China (English Edition), Vol. 26, No. 8, Pp. 2029–2042, 2016, Doi: 10.1016/S1003-6326(16)64321-2.

[18] N. A. Razak, A. H. Ahmad, And M. M. Rashidi, "Thermal Profile and Microstructure of Wrought Aluminium 7075 For Semisolid Metal Processing," International Journal of Automotive and Mechanical Engineering, Vol. 17, No. 2, Pp. 7842–7850, 2020, Doi: 10.15282/Ijame.17.2.2020.03.0584.

[19] S. Farahany, H. R. Bakhsheshi-Rad, M. H. Idris, M. R. Abdul Kadir, A. F. Lotfabadi, And A. Ourdjini, "In-Situ Thermal Analysis and Macroscopical Characterization of Mg–Xca and Mg–0.5ca–Xzn Alloy Systems," Thermochim Acta, Vol. 527, Pp. 180–189, 2012, Doi: Https://Doi.Org/10.1016/J.Tca.2011.10.027.

[20] M. Paradis, M. H. Abdelaziz, A. M. Samuel, F. H. Samuel, And H. W. Doty, "Effect of Mold Type on The Microstructure and Tensile Properties of A356 Alloy," International Journal of Metalcasting, Vol. 11, No. 3, Pp. 523–535, Jul. 2017, Doi: 10.1007/S40962-016-0102-Y.

[21] Sigworth, G.K. Fundamentals of Solidification in Aluminum Castings. Inter Metalcast 8, 7–20 (2014). Https://Doi.Org/10.1007/Bf03355567.

[22] I. Aguilera-Luna, M. J. Castro-Román, J. C. Escobedo-Bocardo, F. A. García-Pastor, And M. Herrera-Trejo, "Effect of Cooling Rate and Mg Content on The Al-Si Eutectic for Al-Si-Cu-Mg Alloys," Mater Charact, Vol. 95, Pp. 211–218, 2014, Doi: 10.1016/J.Matchar.2014.06.009.

[23] N. A. Razak, A. H. Ahmad, And M. M. Rashidi, "Thermal Profile and Microstructure of Wrought Aluminium 7075 For Semisolid Metal Processing," International Journal of Automotive and Mechanical Engineering, Vol. 17, No. 2, Pp. 7842–7850, Apr. 2020, Doi: 10.15282/Ijame.17.2.2020.03.0584.

[24] B. Benjunior, A. H. Ahmad, M. M. Rashidi, And M. S. Reza, "Effect of Different Cooling Rates Condition on Thermal Profile and Microstructure of Aluminium 6061," Procedia Eng, Vol. 184, Pp. 298–305, 2017, Doi: 10.1016/J.Proeng.2017.04.098.

[25] D. Emadi, L. V Whiting, S. Nafisi, And R. Ghomashchi, "Applications of Thermal Analysis in Quality Control of Solidification Processes," J Therm Anal Calorim, Vol. 81, No. 1, Pp. 235–242, 2005, Doi: 10.1007/S10973-005-0772-9.

[26] A. H. Ahmad, S. Naher, And D. Brabazon, "Thermal Profiles and Fraction Solid of Aluminium 7075 At Different Cooling Rate Conditons," In Key Engineering Materials, Trans Tech Publications Ltd, 2013, Pp. 582–595. Doi: 10.4028/Www.Scientific.Net/Kem.554-557.582.

[27] N. H. Husain, A. H. Ahmad, And M. M. Rashidi, "An Overview of Thixoforming Process," In Iop Conference Series: Materials Science and Engineering, Institute of Physics Publishing, Nov. 2017. Doi: 10.1088/1757-899x/257/1/012053.

[28] N. H. Husain, A. H. Ahmad, And M. M. Rashidi, "Thermal Analysis Of 6061 Wrought Aluminium Alloy Using Cooling Curve Analysis-Computer Aided (Cca-Ca) Method," Iop Conf Ser Mater Sci Eng, Vol. 788, No. 1, 2020, Doi: 10.1088/1757-899x/788/1/012018.

[29] H. Jafari, M. H. Idris, A. Ourdjini, And S. Farahany, "In Situ Melting and Solidification Assessment of Az91d Granules by Computer-Aided Thermal Analysis During Investment Casting Process," Mater Des, Vol. 50, Pp. 181–190, 2013, Doi: 10.1016/J.Matdes.2013.02.035.

[30] K. T. Akhil, S. Arul, And R. Sellamuthu, "The Effect of Section Size on Cooling Rate, Microstructure and Mechanical Properties of A356 Aluminium Alloy In Casting," Procedia Materials Science, Vol. 5, Pp. 362–368, 2014, Doi: 10.1016/J.Mspro.2014.07.278.

[31] A. H. Ahmad, S. Naher, And D. Brabazon, "Effects of Cooling Rates on Thermal Profiles and Microstructure Of Aluminium 7075," International Journal Of Automotive And Mechanical Engineering, Vol. 9, No. 1, Pp. 1685–1694, 2014, Doi: 10.15282/Ijame.9.2013.18.0140.

[32] Ihsan-Ul-Haq, J.-S. Shin, And Z.-H. Lee, "Computer-Aided Cooling Curve Analysis of A356 Aluminum Alloy," Metals and Materials International, Vol. 10, No. 1, Pp. 89–96, 2004, Doi: 10.1007/Bf03027368.

[33] X. H. Ma and N. A. Abd Razak, "The Change of Solidification Parameters on Hypoeutectic Aluminum–Silicon Alloy Under Different Cooling Rates," In Technological Advancement in Mechanical and Automotive Engineering, M. Y. Ismail, M. S. Mohd Sani, S. Kumarasamy, M. A. Hamidi, And M. S. Shaari, Eds., Singapore: Springer Nature Singapore, 2023, Pp. 263–278.

[34] M. Rosso, "Thixocasting and Rheocasting Technologies, Improvements Going On," Vol. 54, No. 1, Pp. 110–119, 2012.

[35] S. G. Shabestari and M. Malekan, "Thermal Analysis Study of The Effect of The Cooling Rate on The Microstructure and Solidification Parameters Of 319 Aluminum Alloy," Canadian Metallurgical Quarterly, Vol. 44, No. 3, Pp. 305–312, Nov. 2012, Doi: 10.1179/000844305794409409.

[36] S. Nourouzi, S. M. Ghavamodini, H. Baseri, A. Kolahdooz, And M. Botkan, "Microstructure Evolution of A356 Aluminum Alloy Produced by Cooling Slope Method," In Advanced Materials Research, 2012, Pp. 272–276. Doi: 10.4028/Www.Scientific.Net/Amr.402.272.

[37] V. A. Hosseini, S. G. Shabestari, And R. Gholizadeh, "Study on The Effect of Cooling Rate on The Solidification Parameters, Microstructure, And Mechanical Properties of Lm13 Alloy Using Cooling Curve Thermal Analysis Technique," Mater Des, Vol. 50, Pp. 7–14, 2013, Doi: Https://Doi.Org/10.1016/J.Matdes.2013.02.088.

[38] K. S. Alhawari, M. Z. Omar, M. J. Ghazali, M. S. Salleh, And M. N. Mohammed, "Dry Sliding Wear Behaviour of Thixoformed Hypoeutectic Al–Si–Cu Alloy with Different Amounts of Magnesium," Compos Interfaces, Vol. 23, No. 6, Pp. 519–531, 2016, Doi: 10.1080/09276440.2016.1164496.

[39] I. Aguilera-Luna, M. J. Castro-Román, J. C. Escobedo-Bocardo, F. A. García-Pastor, And M. Herrera-Trejo, "Effect of Cooling Rate and Mg Content on The Al-Si Eutectic for Al-Si-Cu-Mg Alloys," Mater Charact, Vol. 95, Pp. 211–218, 2014, Doi: 10.1016/J.Matchar.2014.06.009.

[40] L. Tian, Y. Guo, J. Li, F. Xia, M. Liang, And Y. Bai, "Effects of Solidification Cooling Rate on The Microstructure and Mechanical Properties of a Cast Al-Si-Cu-Mg-Ni Piston Alloy," Materials, Vol. 11, No. 7, Jul. 2018, Doi: 10.3390/Ma11071230.

[41] S. W. Choi Et Al., "The Effects of Cooling Rate and Heat Treatment on Mechanical and Thermal Characteristics of Al-Si-Cu-Mg Foundry Alloys," J Alloys Compd, Vol. 617, Pp. 654–659, Dec. 2014, Doi: 10.1016/J.Jallcom.2014.08.033.